Energy & Environmental Science

ROYAL SOCIETY OF CHEMISTRY

PAPER

View Article Online
View Journal | View Issue

Cite this: *Energy Environ. Sci.*, 2022, **15**, 4362

Reinforced gel-state polybenzimidazole hydrogen separators for alkaline water electrolysis†

Muhammad Luthfi Akbar Trisno, [ab] Asridin Dayan, [ab] Su Ji Lee,[a] Franz Egert,[c] Martina Gerle, [c] Mikkel Rykær Kraglund, [d] Jens Oluf Jensen, [d] David Aili, [d] Aleksandra Roznowska, [e] Artur Michalak,*[e] Hyun S. Park,[abf] Fatemeh Razmjooei, *[c] Syed-Asif Ansar[c] and Dirk Henkensmeier *[abg]

Received 16th June 2022,
Accepted 1st August 2022

DOI: 10.1039/d2ee01922a

rsc.li/ees

A new membrane fabrication process is presented, in which PBI is cast from a phosphoric acid-based solution and transformed into a KOH doped membrane by immersion in KOH solution. At room temperature, such membranes show a remarkably high conductivity of 300 mS cm^{-1} in 25 wt% KOH solution, 3 times higher than that of conventional PBI membranes cast from DMAc. While swelling of PBI in KOH solution is highly anisotropic, the phosphoric acid-cast membrane shrinks isotropically when immersed in KOH solution, indicating that the ordered, presumably lamellar structures, which are suspected to hinder transfer of ions through the membrane, are transferred into a gel-state. This is further supported by WAXS analysis. DFT calculations suggest that the broad signal in WAXS is related to the distance between hydrogen bonded imidazolides. The soft nature of the KOH doped PBI was mitigated by reinforcement with porous supports. By using a PTFE support, the tensile strength increased from 2 to 32 MPa, and the Young's modulus from 19 to 80 MPa. Immersion in 25 wt% KOH at 80 °C indicated high stability. In the electrolyzer, a conventional PBI membrane failed within 200 hours. In contrast to this, a PTFE-supported separator reached 1.8 A cm^{-2} at 1.8 V and was operated for 1000 hours without failure, which is the longest operation time for ion-solvating membranes to date.

Broader context

Cheap, efficient water electrolysis with non-platinum catalysts is the key to a fossil fuel-free future. The industrial standard is alkaline water electrolysis, which does not require noble metal catalysts (unlike PEM water electrolysis) and uses a highly alkaline feed solution and porous diaphragms to separate anode and cathode. A promising alternative to diaphragms are ion-solvating membranes, like KOH doped PBI. The more dense structure of these membranes potentially reduces gas crossover and may even allow operation at differential pressure, while simultaneously reducing the resistance due to low thickness and high conductivity. However, even though very high performances have been achieved, KOH doped PBI membranes so far failed within 200–300 hours. This work shows a new membrane fabrication process which leads to novel advanced ion-solvating membranes, which have 2 times higher conductivity in comparison to state-of-the art ion-solvating membranes, 10 times lower resistance than commercial Zirfon diaphragms and allowed 1000 hours of failure-free operation in an alkaline water electrolyzer.

1. Introduction

Korea's hydrogen road map foresees that over 17 GW of fuel cells will be installed in Korea until 2040.[1] While some of the required hydrogen fuel can be imported, as much as possible should be produced locally by water electrolysis with renewable energy. At the same time, hydrogen is discussed as one of the most promising media to store renewable energy on a large scale (weeks to months, multi-GWh scale), by using the gas grid, existing gas storage, and underground caverns.[2] In its hydrogen strategy for a climate-neutral Europe, the European Commission estimates that the share of hydrogen in the energy

[a] *Hydrogen Fuel Cell Research Center, Korea Institute of Science and Technology (KIST), Seoul 02792, Republic of Korea. E-mail: henkensmeier@kist.re.kr*
[b] *Division of Energy & Environment Technology, KIST School, University of Science and Technology (UST), Seoul 02792, Republic of Korea*
[c] *Institute of Engineering Thermodynamics, German Aerospace Center (DLR), 70569 Stuttgart, Germany. E-mail: Fatemeh.Razmjooei@dlr.de*
[d] *Department of Energy Conversion and Storage, Technical University of Denmark (DTU), Fysikvej 310, 2800 Kgs. Lyngby, Denmark*
[e] *Department of Theoretical Chemistry, Faculty of Chemistry, Jagiellonian University, 30-387 Krakow, Poland. E-mail: michalak@chemia.uj.edu.pl*
[f] *KHU-KIST Department of Converging Science and Technology, Kyung Hee University, Seoul 02447, Republic of Korea*
[g] *Green School, Korea University, Seoul 02841, Republic of Korea*

† Electronic supplementary information (ESI) available: Computational details, additional WAXS data. See DOI: https://doi.org/10.1039/d2ee01922a

mix will increase from the current 2% to 23% in 2050, and suggests to install 6 GW of renewable hydrogen electrolysers by 2024 and increase that capacity to 40 GW by 2030.[3] Therefore, development of improved and affordable electrolysis systems is required by societies world-wide.

Currently, four different types of systems have reached a mature technological stage or are under development: alkaline water electrolysis (AEL), polymer electrolyte membrane water electrolysis (PEMWE), anion exchange membrane water electrolysis (AEMWE), and solid oxide water electrolysis (SOEC). The latter has energetic advantages, if a source of hot steam is available. PEMWE has a very beneficial performance and high rate capability, but requires platinum and iridium catalysts, which are expensive and scarce.[4] AEL is the most developed technology, which has been used industrially for about 100 years.[5] However, its low rate capability (due to high ohmic resistance) and high gas crossover at differential pressure make it challenging to directly couple it with intermittent renewable energy sources.[6] The preferable system would be an AEMWE, which combines the advantages of AEL (*e.g.* non-platinum group metal catalysts) with those of PEMWE (*e.g.* dense membrane, higher rate capability, use of pure water), but still membranes and an electrode binder which fulfill all requirements (high alkaline stability, high conductivity, high mechanical strength to operate with high differential pressure) are not commercially available.[7]

Traditional AEL uses thick porous diaphragms like AGFA's Zirfon or polyphenylene sulfide fabric (Fig. 1). The effective pore size in Zirfon is reported to be around 150 nm,[8] and the related bubble point is specified by the producer as >2 bar, and it thus prevents the use of Zirfon in electrolysis systems with high differential pressures. In contrast to this, PEMWE and AEMWE use pore-free ion-selective membranes, enabling operation at high differential pressures (*e.g.* 30–100 bar, and a 700 bar target to fit automotive hydrogen tanks[9]). As an example, the hydrophilic clusters in fully hydrated Nafion are in the range of 4 nm, with 1 nm diameter for the bridging areas.[10] Smaller dimensions are expected for less well phase-separated hydrocarbon-based PEM and anion exchange membranes.[11–13]

On the research side, a very promising alternative electrolyte system is KOH doped polybenzimidazole (PBI).[14–24] In contrast to porous diaphragms and phase separated anion exchange membranes, such ion-solvating membranes are separators based on non-porous dense polymer films, which are homogenously swollen by excessive absorption of KOH and water that can support ion conduction. In other words, it behaves like a hydrogel but is not necessarily covalently crosslinked. For O-PBI, a PBI derivative containing an ether linkage as part of the polymer repeat unit, WAXS data indicated an inter-chain distance of *ca.* 0.4 nm.[25] If such a membrane would absorb so much KOH and water that the volume increases 700%, the swelling in each direction (length, width, thickness) would be 100%, and the average distance between chains would double from the initial 0.4 nm to 0.8 nm.

It was shown that the electrolyzer performance with a KOH doped poly(2,2′-(*m*-phenylene)-5,5′-bibenzimidazole) (PBI) membrane can exceed that of a Zirfon based AEL. The cells reach a performance of 1.8 V at 1700 mA cm^{-2} and 630 mA cm^{-2}, respectively, when tested together with highly active non-noble electrodes.[20] This excellent performance was possible even though the PBI membranes in that work had twice lower conductivity, because the denser PBI structure allowed fabrication of membranes with a thickness of just 40–80 μm, which is 8–16% of the thickness of Zirfon. For PBI membranes cast from DMAc and then doped with sulfuric acid, a conductivity of 1–13 mS cm^{-1} has been reported.[26–28] In previous work, we showed that the conductivity of sulfuric acid doped PBI cast from DMAc can be increased to 56 mS cm^{-1} when the membrane is pre-swollen in KOH solution before immersion in the sulfuric acid solution.[29] Most interestingly, Wang and Benicewicz *et al.* reported that a sulfonated *para*-PBI membrane cast from polyphosphoric acid solution and then exchanged into the sulfuric acid form had a conductivity of 593 mS cm^{-1}.[27] Therefore, in this work, we investigate if the conductivity of KOH doped PBI can be increased in a similar way if the membranes are not cast from DMAc, dried carefully (leading to strong polymer–polymer interactions) and then doped with KOH, but if the PBI membranes are dissolved in phosphoric acid, cast into a membrane, washed free from excess acid, and then doped with KOH without any intermediate drying steps. As expected, this process led to much higher conductivities, and the membrane properties and performance in an electrolyzer system are presented.

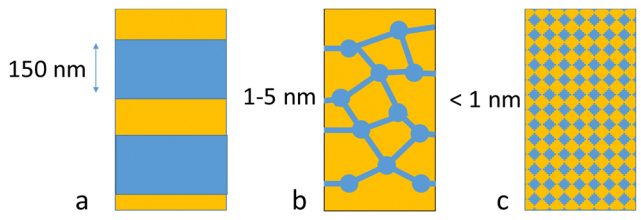

Fig. 1 Illustration of the difference in length scale of the conducting domains in diaphragms (a), phase separated ion exchange membranes (b) and ion-solvating membranes (c). Blue color indicates the water carrying phase, orange the polymer phase.

2. Experimental part

2.1 Materials

PBI fibers (specified as M_w = 58 000 g mol^{-1}) and 40 μm thick PBI membrane were supplied from Blue World Technologies (previously Danish Power Systems). Phosphoric Acid (PA, ACS reagent, 85%) was purchased from Sigma Aldrich. PVDF porous film for support was purchased from Merck Millipore (Durapore Membrane filter DVPP00010, specified as hydrophilic PVDF, pore size 0.65 μm, 125 μm thickness, 70% porosity). Porous Teflon membranes were also obtained from Merck (Omnipore membrane filter JHWP09025, specified as hydrophilic PTFE, pore size 0.45 μm, 65 μm thickness, 80% porosity). Aqueous solutions of potassium hydroxide (KOH) were prepared by dissolving KOH (flakes, Daejung Chemicals and Metal Co., Ltd or pellets, Honeywell) in deionized water.

2.2 Preparation of homogeneous membranes

3 g of PBI was dissolved in 97 g PA in a round-bottom flask (*i.e.* 3 wt% solids) equipped with an overhead stirrer and argon gas purging to evaporate water inside the solution. The solution was stirred at 195 °C for 19 h. After full dissolution, the homogenous solution was poured onto clean glass plates and cast with an automatic casting machine using a doctor blade. The temperature of the glass plate was 60 °C and the casting thickness was 700 μm. The film solidified immediately on the plate and was rapidly dipped into deionized water and stayed immersed for at least 24 h. During that time, the water was several times exchanged. The wet film was cut and immediately equilibrated in an aqueous potassium hydroxide solution with a concentration of 10, 15, 20, 25, or 30 wt% for 24 h at room temperature.

2.3 Preparation of porous supported membranes

PVDF or PTFE porous film was immersed in fully dissolved 3 wt% PBI solution in PA at 150 °C for 1 h. The pore-filled membrane was wiped with tissue paper to remove excess PBI solution on the surface of the membrane and then was immersed in deionized water for at least 24 h with several refreshments. After that, the wet pore-filled membrane was equilibrated in aqueous potassium hydroxide solution, as described above in part 2.2.

2.4 Membrane characterization

Membrane composition was determined by recording the weight fraction of polymer, KOH, and water gravimetrically and the weight fraction of water (WF_{water}), KOH (WF_{KOH}) and polymer ($WF_{polymer}$) was calculated according to eqn (1)–(3), respectively.

$$WF_{water} = \frac{w_{wet} - w_{dry}}{w_{wet}} \quad (1)$$

$$WF_{KOH} = \frac{w_{dry} - w_{dedoped}}{w_{wet}} \quad (2)$$

$$WF_{polymer} = \frac{w_{dedoped}}{w_{wet}} \quad (3)$$

Here, w_{wet} is the weight of a fully doped membrane after being immersed for 24 h in KOH solution and after being wiped with a tissue, w_{dry} is the weight of a membrane dried in a vacuum oven overnight at 80 °C and $w_{dedoped}$ is the weight of a doped and then dried membrane after immersing it in deionized water for at least 24 h, until neutral pH was reached, followed by drying in a vacuum oven overnight at 80 °C. The total electrolyte uptake, KOH uptake and water uptake was calculated according to eqn (4)–(6), respectively.

$$\text{Total uptake} = \frac{WF_{water} + WF_{KOH}}{WF_{polymer}} \quad (4)$$

$$\text{KOH uptake} = \frac{WF_{KOH}}{WF_{polymer}} \quad (5)$$

$$\text{Water uptake} = \frac{WF_{water}}{WF_{polymer}} \quad (6)$$

Shrinking during doping was analyzed by measuring the length and thickness of the casted and water-washed membrane (initial dimension $d_{initial}$) and the KOH doped membrane (wet dimension $d_{KOH\,doped}$). The shrinkage was calculated according to eqn (7).

$$\text{Shrink} = \frac{d_{initial} - d_{KOH\,doped}}{d_{initial}} \quad (7)$$

Conductivity values of doped membranes were obtained by impedance spectroscopy using a Zahner IM6 potentiostat. The membranes were fixed between two gaskets, leaving an active area of 1.767 cm^2. The gap between the electrodes (gold coated copper disc) was 1.59 mm and filled with the respective KOH solution used for doping. The resistance of the membrane was obtained by plotting at least three resistances of stacked membranes (*e.g.* 1–3 samples) against their thicknesses, assuming that the interfacial resistance between two membranes is negligible. The membrane conductivity (σ_m) was calculated according to eqn (8), where slope is the slope of the linear regression of the data points recorded at different membrane thicknesses (resistance per cm).

$$\sigma_m = \frac{1}{\text{slope} \cdot \text{electrode area}} \quad (8)$$

Mechanical properties of membranes were determined with a Cometech Universal Material Testing Machine (model QC-508E). Doped membranes were cut with a blade and for each doped membrane at least 5 samples were tested. The dimensions of the specimen was 10 mm in width, and the distance between the grips was at least 30 mm. The thickness of membranes depended on the doping state and was in the range of 150–200 um. The temperature was 23–25 °C and the relative humidity was 60–65%. The maximum load of the machine was 50 N and the crosshead speed was 10 mm min^{-1}.

SEM images of reinforced mPBI membranes were obtained by FE-SEM Inspect F, 15 kV, after the Pt/Pd sputtering. Cross-sectional images were taken after freeze-breaking samples with liquid nitrogen. SEM energy dispersive spectroscopy (EDS) was employed to acquire atomic distributions.

WAXS spectra were obtained with a Rigaku MiniFlex II with CuKα source in the 2θ range of 10–60° at 4° 2θ min^{-1} scan rate.

Bubble points were measured by punching out a 2.5 cm diameter membrane disc, wetting it in the mentioned solution (water or 25 wt% KOH solution), and assembling it into a filter holder. On one side of the membrane, a pressure was applied and increased over time. The value was measured by a digital manometer. On the low pressure side, a tube was attached, and its open end was immersed in water. The bubble point was noted as the point when bubbles started to emit from the tube.

For determining the membranes' alkaline stability, KOH doped membranes were cut into discs of 3 cm diameter and were then immersed in 25 wt% KOH solution, sealed in polypropylene vials, and kept in an oven at 80 °C. The composition of the samples was analyzed by the gravimetric procedure

described above, using eqn (1)–(3). Total weight loss was calculated by summing up KOH, water, and polymer weight loss.

For the full cell testing, atmospheric plasma sprayed (APS) electrodes of 4 cm^2 active area were used with NiAl as anode and NiAlMo as cathode. The electrodes were produced by spraying powders of NiAl or NiAlMo on nickel mesh by plasma gun from OerlikonMetco (CH) for which Ar was the primary plasma forming gas and H_2 and/or He was used as secondary gases. The spray powder was injected through external injection nozzles into the plasma jet, where particles were accelerated and heated due to momentum and heat transfer between plasma and particles and the quasi or fully molten particles impacted the substrate surface, flattened, solidified and consolidated to form an electrode coating. Multiple layers were coated to form electrodes of suitable thickness. Before the electrochemical test, the porosity was increased by partially leaching out part of the aluminum in KOH solution and some unreacted metals were partially removed in a 30 wt% KOH + 10 wt% NaK-tartrate (complex-former) solutions for 24 h at 80 °C. The zero-gap electrolyzer cell consists of four main parts; stainless steel bipolar plates, Ni wire mesh as gas/liquid diffusion layers, membranes and RANEY® Ni electrodes. Membranes are placed between two electrodes and supported from each side by gas diffusion layers and fixed by stainless steel bipolar plates from both sides. The test has been done in atmospheric pressure in 24 wt% KOH at 80 °C, by recording polarization curves up to 2 A cm^{-2} with a scan rate of 10 mA s^{-1}, after 30 min activation at constant current of 0.2 A using biologic potentiostat. EIS was performed at low and high current densities and plotted from 50 kHz to 100 mHz to identify the ohmic and activation losses. The operating conditions and cell hardware were kept the same for all the tests. The equivalent circuit for fitting consisted of lumped resistance (R_{ohm}) in series with two circuits, each comprising a resistance ($R_{cathode}$ (R_C) and R_{anode} (R_a)) and a constant phase element (CPE1 for cathode and CPE2 for anode) in parallel to each other. The inductor (L) in series with the R_{ohm} represents possible inductive parts of cables and other components. The fitting of Nyquist plot was done by RelaxIS software.

Hydrogen crossover experiments were carried out as separate cell tests. Electrolyte was circulated in both electrolyte compartments at a rate of 80 ml min^{-1}, and the electrolyte circuits were connected in a partially separated mode *via* a *ca*. 20 cm long 1/4″ tube below the degassing vessels but prior to the pumps. The cells were operated at each current density setpoint for 4 hours, with data from the first 30 minutes being discarded to allow for equilibration. Measurements were recorded at 80 °C initially, then followed by 60 °C and 40 °C. A small nitrogen purging flow of 16 ml min^{-1} was fed into the anode degassing vessel, and the exhaust gas was passed through a drying column before reaching an electrochemical hydrogen sensor (Geopal GJ-EX with a Membrapor H2/M-40000 sensor). The sensor was calibrated prior to initial measurements with a 1000 ppm reference gas. Presented results are corrected for the nitrogen fraction, assuming zero humidity and with an oxygen rate on basis of the faradaic current. Specific permeability is calculated from the hydrogen crossover flux values extrapolated to zero current, by linear fitting of data in the range of 50–500 mA cm^{-2}.

3. Results and discussion

3.1 Doping process and membrane composition

PBI can be synthesized by reacting terephthalic acid esters with diamino benzidine in substance at high temperatures.[30] In another widely used process, PBI is synthesized in polyphosphoric acid, and then precipitated in water. To get an organo-soluble material, residual acid is removed by immersion in a mildly alkaline solution.[31] To our knowledge, all previous work on KOH doped PBI membranes used membranes prepared by solution casting from organic solutions (typically DMAc, in one case ethanol/KOH[24]). After complete removal of the solvents, KOH doped membranes were obtained by immersing the pure PBI membranes in KOH solutions. This standard process is displayed in Fig. 2, and the process steps are described by the red unfilled number symbols. In the 3rd step, strong hydrogen bonds between imidazole amine and imine groups can be established, especially when organic solvent traces and absorbed water are carefully removed by drying at elevated temperatures. As a consequence, such treated membranes may require longer doping times to break up again the polymer–polymer interactions, as was recently suggested.[32]

In this work, we investigated a new process, indicated by the filled blue numbered symbols in Fig. 2. Commercial PBI fibers were dissolved in hot phosphoric acid solution, and then cast on a glass plate, forming a membrane when cooled to room temperature. Immersion in water removes the excess acid, so that only the strongly bound acid remains, presumably 1 acid molecule per imidazole group. In this material, the positive charges on the polymer chains, coupled with the high water contents, should efficiently hinder the formation of unwanted strong polymer–polymer-interactions, like the hydrogen bonds which can form between the hydrogen and nitrogen of two neutral imidazole groups. Without drying, these wet membranes were then directly immersed in the KOH doping solutions.

As hypothesized in Fig. 2, washing PA-doped PBI with water only leaches out the excess acid, and about 2 strongly bound acid molecules are expected to remain per repeat unit, unless the washing solution is constantly refreshed (*e.g.* "washing with running water overnight"), which was not the case in this work.[33] Since protonated imidazolium groups and attached biphosphate anions are hydrophilic and interact well with water, and the positive charges on the PBI backbones lead to repulsive forces between the polymer chains, the membranes still contain a lot of water. When these membranes are washed free of remaining, strongly bound PA by immersion in 1 M potassium carbonate, followed by washing with water, the volume shrinking was in the range of about 10% (Fig. 3a). Interestingly, the membranes shrink even further, when they are immersed in KOH solutions. This phenomenon is well-known for ion-exchange membranes, which are impermeable

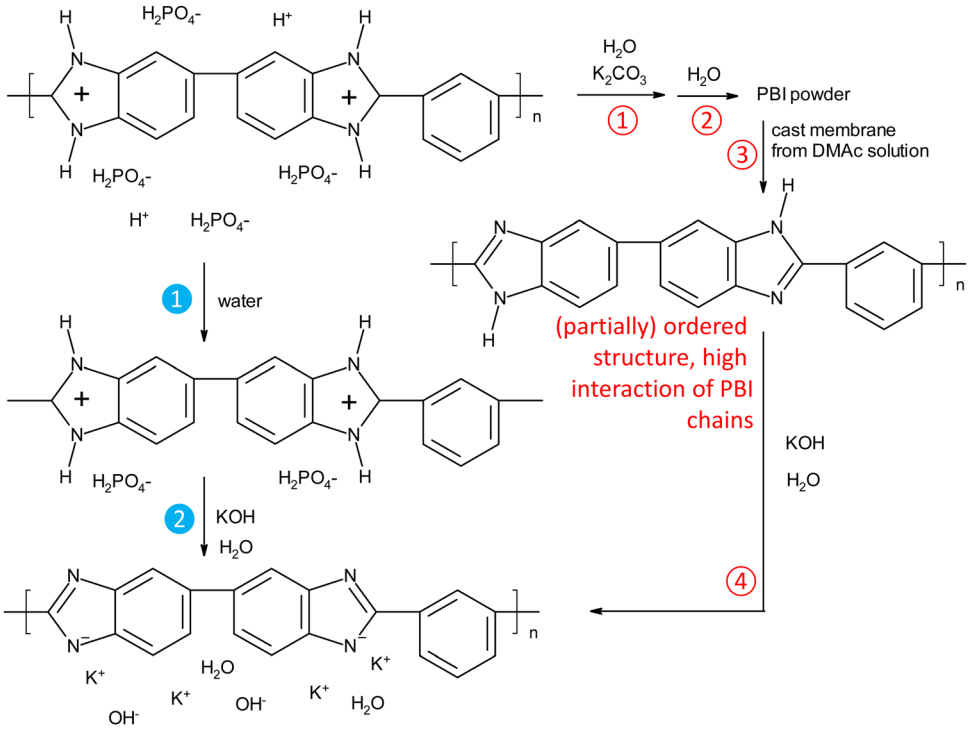

Fig. 2 Chemical structures occurring during the standard preparation process (unfilled red numbered markers) and the alternative preparation process investigated in this work (filled blue numbered markers).

for salts and therefore lose water in contact with salt containing solutions.[34,35] PBI, however, is not a typical ion-exchange membrane, but an ion-solvating membrane; especially at higher concentrations, PBI is highly permeable for KOH, and osmotic pressures can be balanced by exchange of both water and KOH. In fact, for membranes immersed in 10 and 15 wt% KOH, a compositional analysis showed that the formal composition of the absorbed solution is same as the external solution (Fig. 3b). Around 15 wt% KOH, the behavior changes, and the formal composition inside the membrane is higher than in the external solution. A higher concentration of the dopant in the membrane has been previously reported for PA-doped PBI, in which the absorbed PA has a concentration of about 14 M for external concentrations between 3 M and 11 M, due to acid-base interaction between PBI and PA and strong hydrogen bonding interactions between PA molecules.[33]

Doping PBI membranes with PA is typically anisotropic, with a stronger swelling in thickness than in length,[36] and results in an amorphous morphology, in which previous orientations[37,38] are broken. Therefore, when the initially obtained PA-doped amorphous membranes are immersed in water and KOH solution, shrinking should be isotropic. Fig. 3a supports this hypothesis, and shows similar values for length and thickness shrinking from the water washed state to the KOH doped state.

Babcock *et al.* suggested the presence of lamellar structures in PBI membranes cast from DMAc, based on the anisotropic swelling in 25 wt% KOH solution.[38] SANS measurements showed that all structural features vanished within a few hours after immersion in 25 wt% KOH solution, indicating that the lamellar structures break up, and that a re-orientation of the polymer chains occurs.[38] To shed more light on the morphology of KOH doped membranes, XRD measurements for KOH doped membranes were done for PBI membranes cast from (a) DMAc and (b) PA solution (Fig. 4). PBI membranes prepared from DMAc solution and immersed in water or 10 wt% KOH solution show a broad peak around $2\Theta = 24^\circ$. For all other membranes, the main peak is shifted towards $2\Theta = 31^\circ$ (Fig. 4c). According to the Bragg equation, these values refer to dimensions of 3.7 and 2.9 Å, respectively. The first value seems to represent perpendicular spacing between stacked phenyl rings and/or imidazole rings, *i.e.* the inter-segmental distance between polymer chains.[39–41] A shift to higher 2Θ values could indicate closer interaction of the chains, and a shift in the *d*-spacing from 4.0 to 3.6 was reported by Zhu *et al.*, when PBI was doped with small amounts of phosphoric acid.[40] The shift observed in our work is to even narrower structures, from 3.7 to 2.9 Å. Furthermore, SANS proved the absence of larger regularly orientated morphologies in membranes doped at 25 wt% KOH in previous work.[38] Therefore, hypothetically, 2.9 Å could be the distance between potassium ion bridged imidazolide units, for example an amorphous PBI network filled with KOH and water, with ionic interactions of the form $N^-\cdots K^+\cdots N^-$ controlling the swelling of the gel state PBI membrane. To put this in perspective, the distance between two opposite carbon atoms in phenyl groups is in the range of 3 Å.

To investigate more into this, model systems were analyzed by density functional theory (DFT) calculations. The research

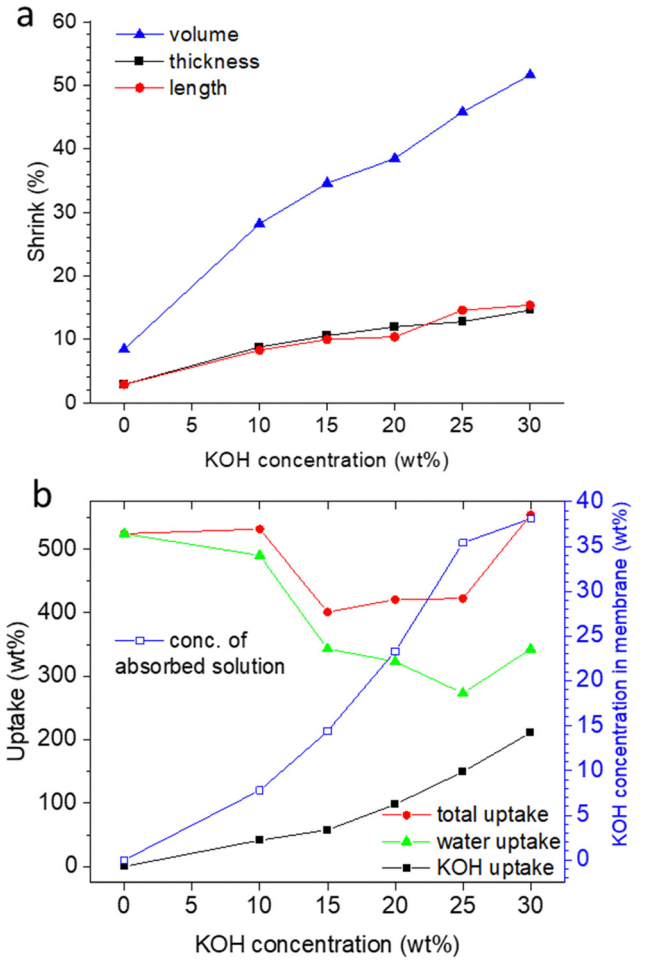

Fig. 3 (a) Dimensional changes when membranes are transferred from the water washed state into the KOH doped state. (b) Composition of KOH doped membranes. Except for KOH uptake in 10 and 15 wt% solution, total uptake in 0 and 15 wt% solution and water uptake in 0 and 15 wt% solution (standard deviations of 16%, 14%, 21%, 11%, 21%, 10% respectively), all data have standard deviations between 0.5 and 6.5%. Before measuring data in 0% KOH, PA was removed by immersion in 1 M potassium carbonate solution.

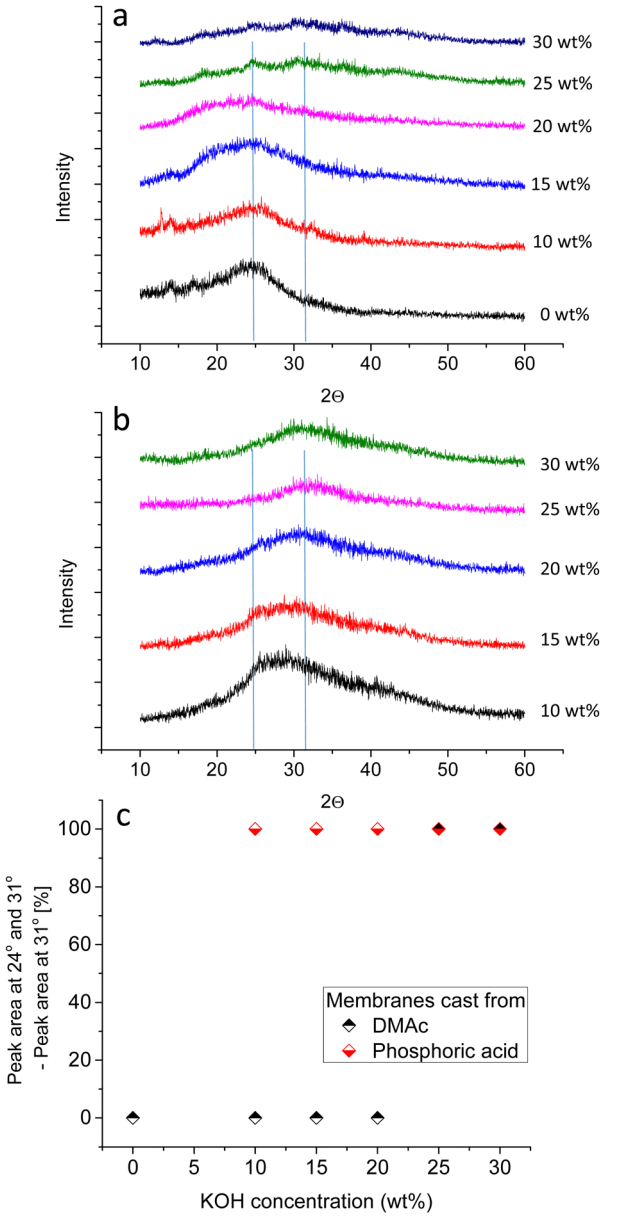

Fig. 4 XRD curves of KOH doped membranes with the concentration of the doping solution indicated; (a) data for membranes cast from DMAc, (b) data for membranes cast from PA, (c) contribution of the peak at 31 degree to the combined peak area at 24 and 31 degree of 2Θ.

was focused on understanding the interactions in systems built of 2, 4, and 8 interacting units of 2-phenylbenzimidazole (**h** fragment), and potassium 2-phenylbenzimidazolide (**k** fragment). In order to explore a large variety of possible structures, a combined computational protocol was used, in which DFT geometry optimizations were performed for the geometries from semiempirical (PM7) molecular dynamics trajectories or Monte-Carlo based structure-generation based approach. Details concerning the models, and methodology can be found in the ESI†.

The results obtained for the models of different size provide a consistent picture, indicating that the most stable structures are characterized by the maximization of π-stacking for K^+ $PBI^-\cdots K^+$ PBI^- (**k–k**) fragments and of hydrogen bonds between $PBI\cdots K^+$ PBI^-(**h–k**) fragments. More importantly, it was found that N–N distances are substantially longer than 3.1 Å in the absence of hydrogen bonding (*i.e.* $N^-\cdots K^+\cdots N^-$). However, distances in the range of 2.7–2.9 Å were found for hydrogen-bonded systems, in which imidazole units interact with potassium imidazolide units. Also, π-stacking was observed in the most stable (lowest energy) model structures (see Fig. 5 and ESI†).

Based on these results, it can be hypothesized that only 50% of PBI units are deprotonated in fully KOH doped membranes, leading to hydrogen-bonded imidazole···imidazolide fragments, in which each imidazole-based system bears a half negative charge. This actually could explain why the conductivity of PBI doped in 25 wt% KOH was reported to be in the range of 90 mS cm^{-1} in ref. 21, even though compositional analysis by prompt gamma activation analysis (PGAA) and titration showed K/N ratios of 0.5–0.6 in ref. 38, *i.e.* fully

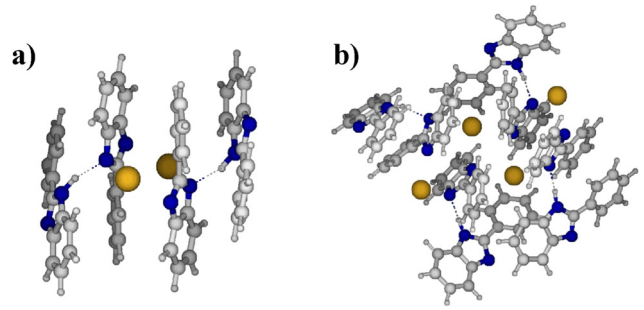

Fig. 5 DFT-lowest-energy structures, exhibiting both, hydrogen bonding, and π-stacking, in the model systems built of 4 (part **a**) and 8 (part **b**) **h**/**k** units, with **h** : **k** ratio equal 1 : 1. In the structures presented, the shortest distances between nitrogen atoms are 2.84 Å and 2.83 Å, for 4 and 8 units, respectively.

deprotonated PBI consisting formally of potassium/imidazolide ion pairs, which may not have a high conductivity: The same K/N ratio would also be observed, if the actual structure is more like $K^+\cdots$imidazolide$\cdots H^+\cdots$imidazole$\cdots K^+\cdots OH^-$.

In conclusion, XRD data reveals that the ordered structures are broken up even at lower KOH concentrations for membranes prepared from PA solution, and that these membranes are gel-state membranes, possibly with hydrogen bonded imidazole/potassium imidazolide units and excess dissociated KOH.

3.2 Membrane conductivity and mechanical properties

Conductivity was tested for several membrane samples in KOH solutions having the concentrations of 10, 15, 20, 25 and 30 wt% KOH (Fig. 6a). For the gel-state membranes cast from PA, the conductivity was significantly higher than that of PBI membranes conventionally cast from DMAc solutions, and reached 300 mS cm^{-1} in 25 wt% KOH solution. For comparison, the conductivity of a commercial Zirfon membrane was 204 mS cm^{-1} at the same conditions. Considering the thickness of Zirfon (500 μm) and PBI (185 μm, but adjustable within a certain range), the resulting area specific resistances, which contribute to the cell resistances in an electrolyzer, are 245 and 62 mΩ cm^2, respectively.

The experimental variation of the measured conductivity values was relatively large. This was presumably due to a variation in the thickness measurement, because soft, fully swollen membranes are easily compressed by the thickness gauge. The samples were kept in the doping solutions and the conductivity was re-measured after an additional 4 to 8 weeks. Interestingly, there was a slight trend towards increasing conductivity over time, indicating that the membranes continue to absorb solution, although at a very slow rate. This observation also suggests that membranes are stable at room temperature in KOH solution.

Fig. 6b compares the average conductivity of PA-cast PBI membranes with that of standard PBI prepared from DMAc, and the dependence of the conductivity on the formal concentration of the absorbed solution and its amount. Similar to PA doped membranes, which often show an exponential increase of conductivity with the PA uptake,[42] the strongest effect on conductivity is seen by the uptake of absorbed KOH solution.

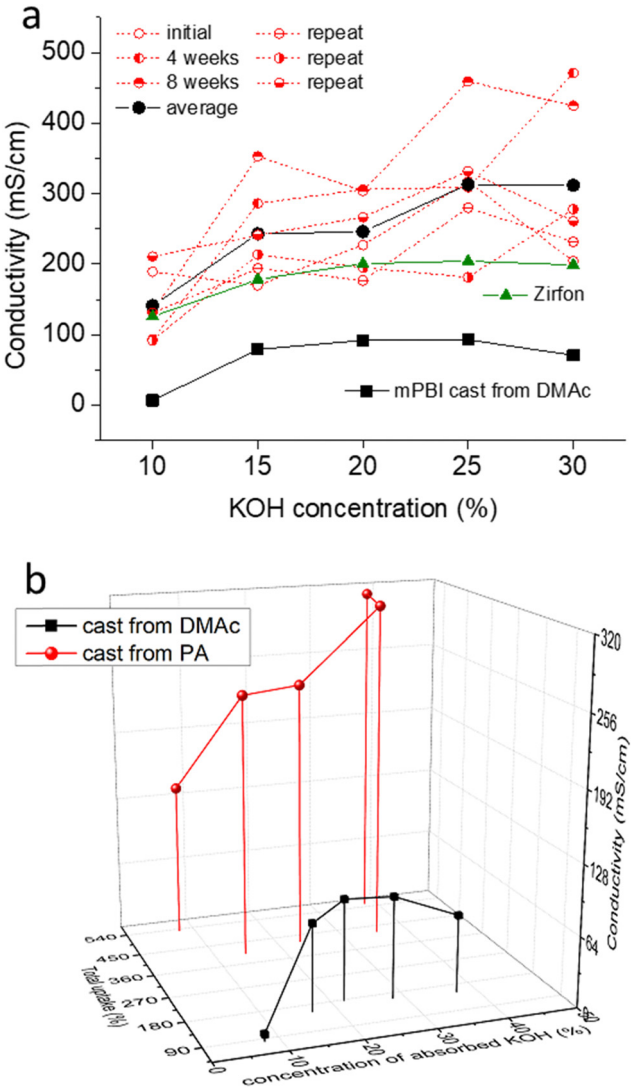

Fig. 6 Conductivity of KOH doped PBI membranes at room temperature, and its dependence on KOH concentration (a) and total absorbed solution and formal concentration of the absorbed solution (b); 4 weeks and 8 weeks indicates the time for which membranes aged in the doping solution; repeat is data for a new set of membranes; data for PBI cast from DMAc solution was taken from our previous work.[21]

PBI is a strong material, and has a tensile strength above 100 MPa and Young's modulus in the range of 1–2 GPa. The exact properties of a specimen depend on its hygro-thermal history, which impacts the degree of hydrogen bonding, entanglement, degree of crystallization, and water contents. All gel membranes showed dramatically decreased tensile strength and Young's modulus (Table 1). From a practical perspective, this decrease is partially compensated by an increased elongation at break, *i.e.* already small stresses result in deformation, but only large strain results in membrane failure.

3.3 Membranes with a porous support

To improve the mechanical strength of the membranes and limit potential issues which may arise from compression, like creep or leaching of KOH solution from the compressed

Table 1 Mechanical properties of KOH doped membranes. For 0 wt% KOH solution, strongly bound PA was removed from the membrane by first immersion in water, then in carbonate solution and then again in water

KOH concentration in doping bath (wt%)	Tensile strength (MPa)	Young's modulus (MPa)	Elongation at break (%)	Toughness (MPa)
Commercial PBI membrane, cast from DMAc, water swollen	100.8 ± 9.1	1285 ± 160.6	22.4 ± 3.2	17.5 ± 1.9
0	2.38 ± 0.13	33.0 ± 4.0	22.1 ± 6.6	0.30 ± 0.07
10	1.40 ± 0.11	14.8 ± 2.3	90.4 ± 35.8	1.27 ± 0.32
15	1.90 ± 0.10	17.3 ± 0.7	145.7 ± 17.5	2.03 ± 0.23
20	1.92 ± 0.27	19.6 ± 9.2	104.2 ± 38.4	1.75 ± 0.02
25	2.24 ± 0.43	18.8 ± 1.2	122.3 ± 43.8	2.57 ± 0.63
30	2.25 ± 0.03	23.1 ± 1.8	142.3 ± 4.4	2.16 ± 0.09

membrane, a porous support material was introduced. At this point, the main consideration was to have access to a commercial porous membrane, which (a) is thick enough to limit gas crossover, (b) does not swell noticeably in contact with water-based solutions and (c) which can be wetted by PA solutions containing PBI. These requirements were fulfilled by Merck Millipore's Durapore Membrane filter DVPP00010, which is specified as a hydrophilic PVDF, and has a pore size of 0.65 μm, 125 μm thickness, and 70% porosity.

The expected drawback is that PVDF degrades under alkaline conditions, by elimination of HF, leading to the formation of C═C double and maybe triple bonds, which can undergo further reactions.[43] When membrane samples were immersed in 25 wt% KOH solution at 60 and 80 °C, indeed a slight discoloration of the solution was visible, and the color of the membrane changed from white (pristine) to brown (60 °C) to black (80 °C) within 2 days. However, the membrane appeared to be intact and did not break.

Pore filling was done by first dissolving PBI in PA at 150 °C, and then immersing a porous PVDF membrane in that solution for 1 hour. After that, the same process steps were applied, as for pure PBI membranes cast from PA solution. During this process, the white PVDF membrane turned into the amber color typical for PBI membranes, indicating that pore filling with PBI was successful (Fig. S6e and f, ESI†). Cross-sectional SEM images of pristine and pore-filled PVDF showed a significant decrease of the porosity during pore filling (Fig. S6a and b, ESI†). The membranes do not appear dense in the SEM images. This is related to the high water contents, which is 52 wt% for pure PBI equilibrated in 25 wt% KOH solution (see Fig. 3b). Therefore, when contacted with 25 wt% KOH solution, it can be assumed that most pores are closed, and that remaining pores are dead-ended and do not offer a pathway for gases through the membrane. SEM EDS (Fig. S6d, ESI†) proved that PBI was fairly well distributed over the whole membrane area, except for a few domains which appear to be less doped.

Because PVDF reacts with concentrated KOH solutions, also membranes using hydrophilic expanded Teflon membranes as reinforcement were prepared (Fig. 7). It should be stressed that SEM measurements are done in the vacuum, and that the pores visible in Fig. 7 may actually be formed when the gel-type PBI in the pores loses water and shrinks. Reinforcement with porous PTFE increased the tensile strength from 2 MPa for the unsupported membrane to 32 MPa for the non-reinforced membrane

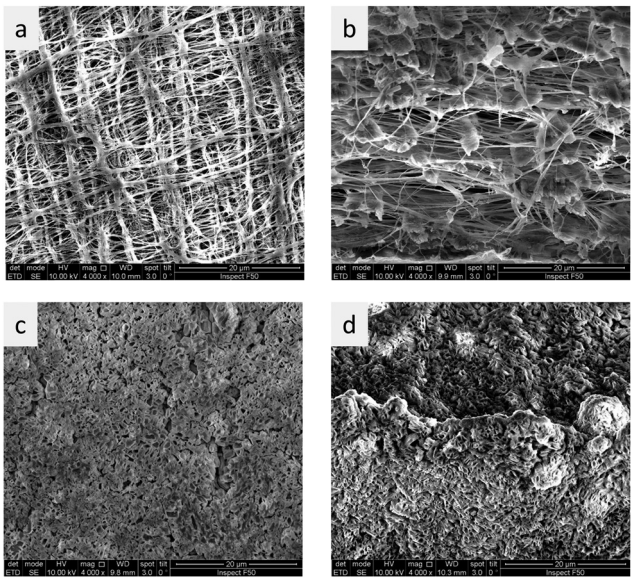

Fig. 7 SEM images of Teflon membrane before (a and b) and after pore filling with PBI (c and d); a and c are surface images, b and d are cross sectional images; for all images, the scale bar represents 20 μm.

(Table 2). It should be noted that tensile strength is a material property, and that the real resistance to external stresses in the application is influenced by the material dimensions. For example, Zirfon has a tensile strength in the range of 2 MPa (1.8 MPa,[44] 2.1 MPa[45]). This means that a membrane stripe of 1 cm width will break at a stress of 10 N (= 2 MPa × 0.5 mm × 10 mm). In contrast to this, a 65 μm thick PTFE/PBI membrane will break at a stress of 21 N.

The assumption that the pore-filled PVDF membranes are gas tight was supported by bubble point measurements. Commercial Zirfon membranes are specified by AGFA do have a bubble point above 2 bar. In our test setup, the maximal applicable pressure was 5.6 bar. As shown in Table S1 (ESI†), porous PVDF showed a bubble point of 2.4 bar when wetted with KOH solution. In other words, at a pressure of 2.4 bar, the pressure was sufficient to push the KOH solution out from the membrane pores, and a constant flow of gas was observed. For both AGFA Zirfon and PVDF/PBI, the bubble point was larger than 5.6 bar and could not be observed with the experimental setup. This result does not allow to draw conclusions regarding the permeability of the membranes, but suggests that the

Table 2 Properties of supported membranes doped in 25 wt% KOH, and comparison with the homogenous membrane material

	Tensile strength (MPa)	Young's modulus (MPa)	Elongation at break (%)	Toughness (MPa)	Conductivity (mS cm^{-1})	Thickness (μm)	ASR (mΩ cm^2)
Without support	2.2 ± 0.4	18.8 ± 1.2	122.3 ± 43.8	2.57 ± 0.63	313 ± 90[a]	185	64 ± 21[a]
PVDF/PBI	5.5 ± 0.4	104.9 ± 6.9	31.2 ± 1.5	1.37 ± 0.08	221.5 ± 34.3	113	51 ± 8
PTFE/PBI	32.2 ± 2.5	79.9 ± 4.9	96.0 ± 4.0	18.8 ± 1.12	247.7 ± 7.7	65	25 ± 1

[a] See Fig. 6 and explanations there for the high standard deviation.

pore-filled PVDF membranes are intrinsically safe to test in AEL, because pressure fluctuations will not lead to instant mixing of hydrogen and oxygen.

3.4 Alkaline stability

Alkaline stability of gel-state mPBI membranes was evaluated in 25 wt% KOH solution at 80 °C. The weight of the KOH doped membranes decreased by around 30% within the first 12 hours and then decreased further to 35% weight loss over the next 7 days. GPC analysis revealed that Mw increased 6%, while the polydispersity decreased from 3.19 to 3.01 (Table S2, ESI†). This clearly shows that no chain scission occurred, and indicates that low molecular weight fractions leached from the membrane sample. However, this loss hardly influenced the sample weight: analysis of the membrane composition revealed that this loss originates from loss of water and KOH (Fig. 8a). Interestingly, both water and KOH uptake decrease 40%, so that the formal composition of the absorbed solution remains constant. In another experiment, weight loss was monitored over the time of 4 weeks (Fig. 8b). It can be seen that reinforced membranes have lower weight losses, possibly because the support hinders shrinking. These results indicate that mPBI does not degrade chemically, but that the membrane experiences a physical equilibration. This is also supported by visual inspection that the color of aging PBI membranes and the KOH solution are unchanged, *i.e.* no PBI was lost to the solution. However, a discoloration was observed for PVDF membranes, because PVDF is not alkaline stable.

The loss of electrolyte is expected to result in reduced conductivity. For this purpose, the through-plane conductivity of a gel-state mPBI membrane was tested at room temperature before and after heating for 1 day to 80 °C in 25 wt% KOH solution. The heat treatment reduced the conductivity of the analyzed sample from initially 425 mS cm^{-1} to 306 mS cm^{-1}, a decrease by 28%, which (we assume coincidentally) is directly proportional to the amount of the leached-out electrolyte quantity. XRD spectra of membranes before and after heating show no shift in the peaks which would lead to a different semi-crystalline structure (Fig. S5, ESI†).

The weight loss of the PVDF/PBI membrane was in the range of 10% after 4 weeks. This value is expected, because the porosity of the porous PVDF membrane is specified as 70%; *i.e.* 35% weight loss of the water/KOH phase will lead to a total weight loss of 10.5% for PVDF/PBI. The weight loss of the PTFE/PBI membrane should have been less, because porosity of the PTFE is 80%, but unexpectedly was a bit higher. This could be related to the different production processes of porous PVDF and porous PTFE membranes. Porous PVDF is usually produced by phase inversion, while porous PTFE is extended in x and then y direction, which results in stresses which could be released at higher temperatures, and thus change the porosity.

For comparison, we also tested the alkaline stability of a commercial Zirfon membrane. Since this membrane is a porous membrane based on rigid, hydrophobic polysulfone, no weight loss was expected. Indeed, when the membrane was equilibrated in 25 wt% KOH at room temperature, the weight increased slightly when the temperature was increased to 80 °C, and the weight gain remained in the range of 0.9 ± 0.4% for the test time of 4 weeks.

3.5 AEL test and crossover

PTFE/PBI and PVDF/PBI membranes along with the electrodes (NiAl as an anode and NiAlMo as a cathode) were implemented

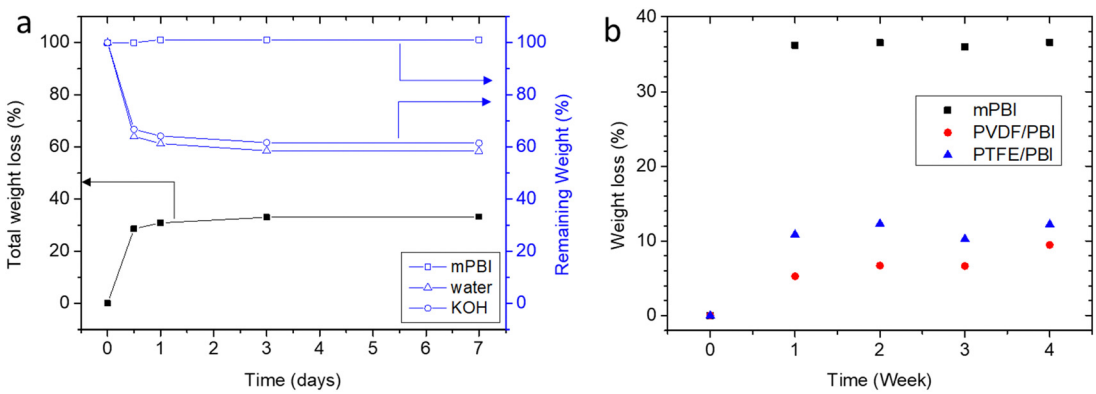

Fig. 8 Stability of membranes in 25 wt% KOH solution at 80 °C; (a) total weight loss over 7 days and remaining portion of PBI, KOH, water; (b) total weight loss over 4 weeks.

in the AEL cell to investigate the effect of membranes on the cell performance. For comparison, one cell was also assembled with a commercial PBI-based membrane with the same electrodes and tested under the same conditions.

Fig. 9a shows the polarization curves of the AEL cells with the PTFE/PBI, PVDF/PBI and commercial membranes, all using the same electrodes operated in atmospheric pressure in 24 wt% KOH at 80 °C. The efficiency increases from 77 and 79% HHV for the cell with commercial PBI membrane and PVDF/PBI membrane, respectively, to 80% HHV for the cell with PTFE/PBI membrane. The cell with the PTFE/PBI membrane displays the highest rate capability of approximately 1.79 A cm^{-2} at 1.8 V. The cell with the PVDF/PBI membrane shows a rate capability of 1.76 A cm^{-2} at 1.8 V and the cell with commercial PBI membrane shows a rate capability of 1.62 A cm^{-2} at 1.8 V. Although these results show that all membranes show more or less similar performance, a slightly lower cell voltage at a given current density is still observed for the AEL with PTFE/PBI. However, even this result obtained by PTFE/PBI membrane is exceeding what has previously been achieved with membranes in alkaline environments (*e.g.* 630 mA cm^{-2} for a similar cell with Zirfon membrane),[20] and is comparable to state-of-the-art PEMWE. A comparison of the performances of different representative AEL and AEMWE systems is given in Fig. S12 (ESI†). Electrochemical impedance spectroscopy (EIS) was carried out to investigate further the effect of using different membranes in alkaline solution. Fig. 9b and c show the impedance analysis together with their model fits as a Nyquist plot for different membranes at very low and high current densities of 0.05 and 1.75 A cm^{-2}. The equivalent circuit (Fig. S7a of ESI†) consisted of ohmic resistance R_{ohm} in series with two circuits, each comprising a resistance R_c for cathodic reaction and R_a for anodic reaction. The R_{ohm} or high frequency resistance, which appears as the intercept of the Nyquist plots with the *x*-axis at high frequency (left side of Nyquist plot) represents the total internal ohmic resistance of the cell, which arises mainly from solution and membrane resistance and partially contact resistance. The polarization resistance, R_c and R_a, are identified with the cathode and anode activity.[46] The impedance data collected at low current density 0.05 A cm^{-2} (Fig. 9b) show that all the cells with different membranes have almost similar ohmic and charge transfer resistance, which is in line with the polarization curves. In detail, the resistances were R_{ohm} = 0.014, R_c = 0.013, R_a = 0.18 Ω

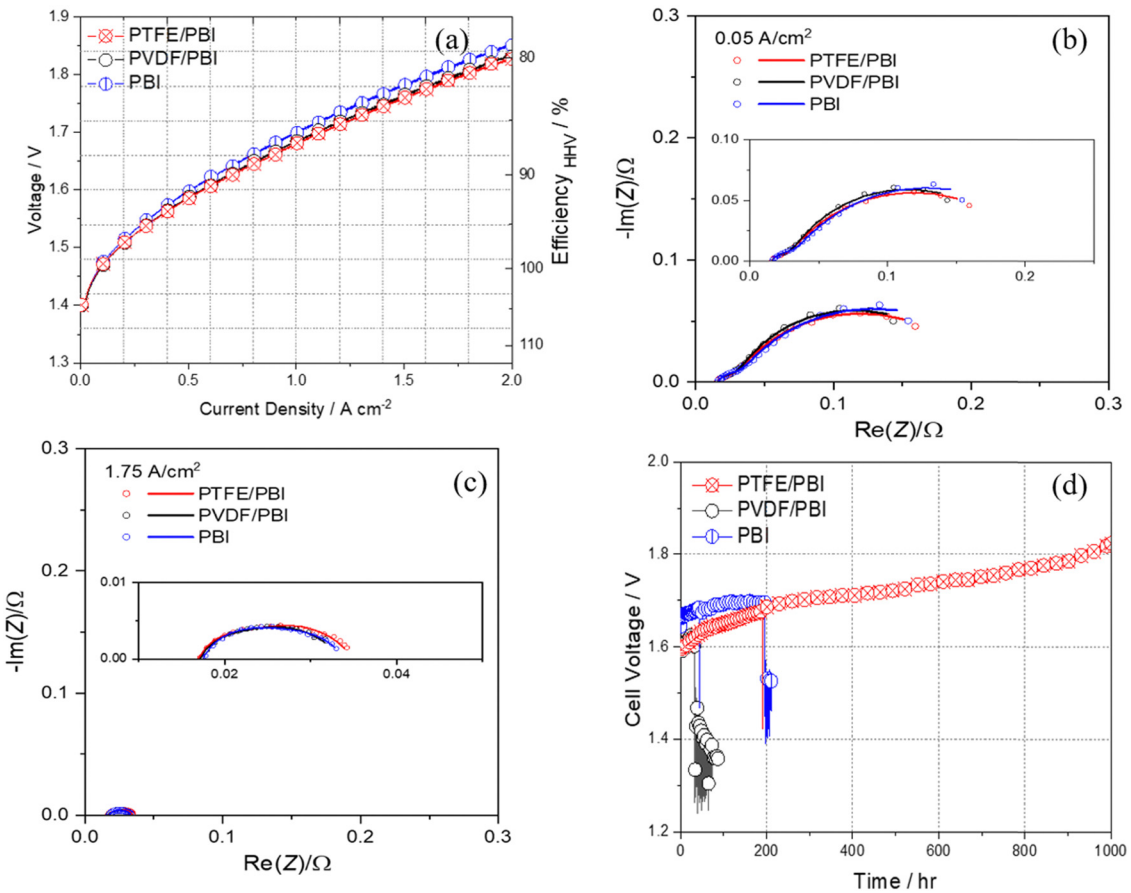

Fig. 9 Electrochemical characterization of the AEL cell with RANEY® Nickel electrodes, with PTFE/PBI, PVDF/PBI and commercial PBI membranes in 24 wt% KOH at 80 °C: (a) cell–voltage curves, not corrected for *iR* (b) Nyquist plots from the EIS measurements and their fittings for cells with different membranes at 0.05 A cm^{-2} and (c) at 1.75 A cm^{-2}, the magnified Nyquist plots are shown in the inset and (d) chronoamperometric measurements at a constant current density of 0.5 A cm^{-2} for all three cells with different membranes.

for PTFE/PBI, R_{ohm} = 0.015, R_c = 0.014, R_a = 0.17 Ω for PVDF/PBI and R_{ohm} = 0.015, R_c = 0.016, R_a = 0.19 Ω for PBI. The same behavior has been observed at higher current density of 1.75 A cm^{-2} (Fig. 9c), and resistances were R_{ohm} = 0.015, R_c = 0.007, R_a = 0.012 Ω for PTFE/PBI, R_{ohm} = 0.015, R_c = 0.007, R_a = 0.012 Ω for PVDF/PBI and R_{ohm} = 0.016, R_c = 0.006, R_a = 0.011 for PBI.

The durability of cells with PTFE/PBI, PVDF/PBI, and commercial PBI membranes in 24 wt% KOH was evaluated under a constant current density of 0.5 A cm^{-2} at 80 °C, and the cell–voltage changes as a function of test time are shown in Fig. 9d. The PVDF/PBI membrane-based cell failed after 32 hours continuous operation due to inadequate stability of PVDF in alkaline conditions. The cell with the commercial PBI membrane failed after 196 hours constant operation. However, the PTFE/PBI membrane-based cell was successfully operated for 1000 hours and showed a 230 mV increment in cell voltage at end of operation. The PTFE/PBI membrane remained visually unchanged after durability test (Fig. S8, ESI†), whereas PVDF/PBI and commercial PBI membranes showed cracks after disassembly. This result reveals that the PTFE/PBI membrane is quite stable for a long duration of 1000 hours, which is the first such report in the existing literature on such high stability for alkaline PBI-based ion solvating membranes. Fig. S7b and c (ESI†) show the impedance analysis together with their model fits as a Nyquist plot for the cell with PTFE/PBI membrane at the begin and end of test at very low and high current density of 0.05 and 1.75 A cm^{-2}. At 0.05 A cm^{-2}, where charge transfer resistance is the most dominant factor for the total cell performance, an increment in charge transfer resistance was observed; at the end of test, this was R_c = 0.039 and R_a = 0.23 Ω. Since it is not expected that degradation is significant at such a low current density we attribute the activation loss to the bubble formation, coalescence of bubbles and thus augmentation in the bubble size on the electrode surface and partially active sites blockage leading to increase of activation loss at low current density.[47] The ohmic loss results from membrane and contact resistance. The same increment in ohmic loss (0.026 Ω) at 0.05 A cm^{-2} could be more related to the formation of bubble and the trapped bubbles between the electrode surface and membrane leading to decreased contact area. At 1.75 A cm^{-2}, where ohmic resistance is the most dominant factor for the total cell performance, almost no changes in charge transfer resistance were observed for the cell with PTFE/PBI membrane after 1000 h test (R_c = 0.007 and R_a = 0.013 Ω). It is reported that the increase of current density brings down the critical diameter for bubble formation and causes the bubble release from the electrode surface.[47] Very high current densities can result in two possible effects. The high voltage applied would result in local heating stemming from the ohmic loss at higher current densities. This localized heating in turn causes a temperature gradient formation on the electrode surface. Although more gas is formed at higher current density, the localized heating might cause a reduction of the bubble size and thus assist in releasing the bubbles from the electrode surface.[47] Moreover, at higher current densities, where gases are formed at higher rates, bubble detachment is more effective and a well separated gas distribution over the electrode surface may develop. At higher current densities enough driving force is applied to reduce the bubble coverage on the porous electrode surface, and in turn no changes in activation loss was observed before and after durability test. However, the ohmic loss increased for PTFE/PBI membrane over the duration of the test (final R_{ohm} = 0.027 Ω), which can be due to slight physical changes of the membrane (*e.g.* compression of the porous structure with related loss of KOH and water *etc.*), which can be observed from Fig. 9d. However, such durability without failure is the longest operation time reported for ion-solvating membranes to date. Some more works will be done in future for increasing the stability of the PTFE/PBI membrane (*e.g.* by crosslinking) while still keeping the high performance.

After the electrolyzer test, the PTFE/PBI membrane was analyzed optically (Fig. S8, ESI†) and by XPS (Fig. S10 and S11, ESI†). Although the anode side had a higher PTFE/PBI ratio than the cathode side, this could be due to creep, partial dissolution, or simply a different initial coating thickness. Most importantly, no additional peaks indicating N–O or C═O were found.

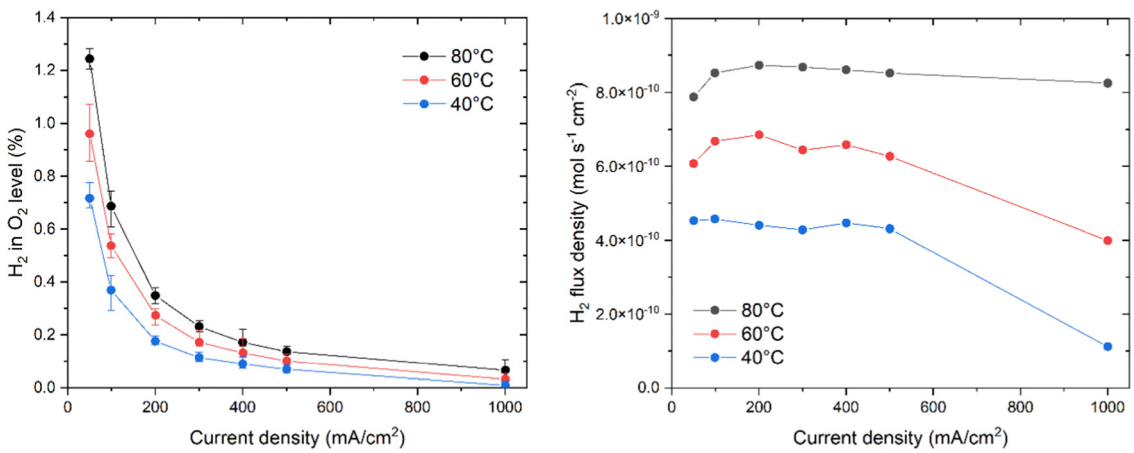

Fig. 10 Hydrogen crossover. Hydrogen-in-oxygen levels (a), and hydrogen crossover flux density (b). Measured in 24 wt% KOH. The low values at 1000 mA cm^{-2} have large relative errors as they are close to the setup's sensitivity.

The hydrogen crossover behavior was measured for the PTFE/PBI membrane, and Fig. 10a shows the measured average hydrogen-in-oxygen levels as a function of current density, when corrected for the nitrogen purging flow. The error bars represent the highest and lowest values recorded for the given data point. The trend is very close to expected constant diffusion based behavior, for which the increased dilution with oxygen at increasing currents results in overall lower levels. While the hydrogen level values at 50 and 100 mA cm^{-2} might seem high at first glance, we note that the PTFE/PBI membrane was only 65 μm thick, and thus it can be more helpful to consider the hydrogen flux density, or the equivalent specific permeability. Fig. 10b shows the hydrogen crossover flux density, and the observed values are seemingly independent on current density. This suggests that the crossover is purely diffusion driven, and that the local oversaturated concentration does not increase with current for these specific electrodes. This is slightly different from the weakly increasing trends observed in other works.[48] Similar graphs for Zirfon and a commercial PBI membrane are available in the ESI.† Specific permeability was calculated by extrapolating the 50–500 mA cm^{-2} data to zero current, and found to be 3.0, 4.2, and 5.4 × 10^{-12} mol s^{-1} cm^{-1} bar^{-1} at 40, 60 and 80 °C respectively. This is lower than for PBI (4.0, 5.1, and 6.8 × 10^{-12} mol s^{-1} cm^{-1} bar^{-1}) as well as Zirfon (15, 25, and 28 × 10^{-12} mol s^{-1} cm^{-1} bar^{-1}). For comparison, literature reports specific permeabilities of 5.3, 7.3, and 26.4 × 10^{-12} mol s^{-1} cm^{-1} bar^{-1} for A201, FAA3 and N117 membranes, which is all higher than that of PTFE/PBI membranes.[49]

4. Conclusions

A new membrane casting process was developed, in which PBI is first dissolved in hot PA and cast into a wet film, which quickly solidifies at room temperature. Immersion in water removes most of the acid, and redoping with KOH solution leads to a dense PBI membrane which can be used in AEL. In contrast to conventionally (from DMAc solutions) cast membranes, the acid-cast membranes have a larger free volume and thus much increased uptake of KOH and water. This leads to about three times higher conductivity of 310 mS cm^{-1}. The drawback is a low tensile strength and Young's Modulus. Reinforcing with a porous PVDF support slightly improves the mechanical properties, but PVDF degrades under the harsh alkaline conditions of the electrolyzer. Reinforcing with a porous PTFE support increases the tensile strength by a factor of 16 to 32 MPa, and the toughness by a factor of more than 7. Furthermore it was shown that the KOH doped PBI is chemically stable under alkaline conditions. A weight loss of about 30–35% is observed within the first hours in contact with 25 wt% KOH solution at 80 °C, but was shown to stem from loss of water and KOH at the elevated temperatures. PTFE reinforced membranes show even lower weight loss, presumably because the porous support prevents shrink of the KOH doped PBI matrix.

Both supported membranes achieved a record-high performance in the noble metal-free electrolyzer of close to 1.8 A cm^{-2} at 1.8 V in 24 wt% KOH solution at 80 °C, comparable to state-of-the art PEM electrolyzers using platinum group catalysts. While the PVDF/PBI membrane failed within just a few hours, due to the poor alkaline stability of PDVF, the PTFE supported membrane showed a remarkably stable performance at 500 mA cm^{-2} over the test time of 1000 hours.

Further work should focus on two directions: first, optimization of the porous support, to find a material of higher glass transition temperature than PTFE, identify optimal thickness, and to optimize the porosity and wettability of the support and thus the pore filling process. Second, optimization of the PBI chemistry, *i.e.* to test the effect of different backbone chemistries, side groups and crosslinks on the PBI performance and resistance to aging.

We believe that the new material class developed in this work will open a way towards using AEL in combination with intermittent renewable energy and at low differential pressures.

Author contributions

Muhammad Luthfi Akbar Trisno – investigation, visualization, writing – original draft; Asridin Dayan – investigation, visualization; Su Ji Lee – investigation; Franz Egert – investigation; Martina Gerle – investigation; Mikkel Rykær Kraglund – investigation, writing; Jens Oluf Jensen – funding acquisition, project administration, writing – review and editing; David Aili – funding acquisition, project administration, writing – review and editing; Aleksandra Roznowska – investigation, visualization, writing – original draft; Artur Michalak – validation, supervision, writing – review and editing; Hyun S. Park – resources, supervision, writing – review and editing; Fatemeh Razmjooei – supervision, visualization, writing – original draft; Syed-Asif Ansar – resources, writing – review and editing; Dirk Henkensmeier – conceptualization, project administration, supervision, writing – original draft.

Conflicts of interest

There are no conflicts to declare.

Acknowledgements

KIST: this work was supported by KIST internal project, as part of unfunded participation in the EU project ''NEXTAEC''. DLR, DTU: this project has received funding from the European Union's Horizon 2020 research and innovation program under grant agreement No. 862509 (''NEXTAEC''). Jagiellonian University: We thank the PL-Grid Infrastructure and the Academic Computational Centre Cyfronet of the University of Science and Technology in Krakow for providing computational resources. AR has been partly supported by the EU Project POWR.03.02.00-00-I004/16.

References

1 https://english.hani.co.kr/arti/english_edition/e_business/879097.html, assessed 2021.09.13.

2 L. Lankof and R. Tarkowski, Assessment of the potential for underground hydrogen storage in bedded salt formation, *Int. J. Hydrogen Energy*, 2020, **45**, 19479–19492, DOI: **10.1016/j.ijhydene.2020.05.024**.

3 European Commission, Communication from the commission to the European Parliament, the council, the European economic and social Committee and the committee of the regions – A hydrogen strategy for a climate-neutral Europe, Brussels, 8.7.2020, **https://ec.europa.eu/energy/sites/ener/files/hydrogen_strategy.pdf**, last assessed 2021.08.09.

4 M. Carmo, D. L. Fritz, J. Mergel and D. Stolten, A comprehensive review on PEM water electrolysis, *Int. J. Hydrogen Energy*, 2013, **38**, 4901–4934, DOI: **10.1016/j.ijhydene.2013.01.151**.

5 J. O. Jensen, C. Chatzichristodoulou, E. Christensen, N. J. Bjerrum and Q. Li, Intermediate temperature electrolysers, in *Electrochemical Methods for Hydrogen Production*, ed. K. Scott, Energy and Environment Series, No. 25, Royal Society of Chemistry, ch. 7, 2020, pp. 253–285, DOI: **10.1039/9781788016049**.

6 Y. Guo, G. Li, J. Zhou and Y. Liu, Comparison between hydrogen production by alkaline water electrolysis and hydrogen production by PEM electrolysis, *IOP Conf. Ser.: Earth Environ. Sci.*, 2019, **371**, 042022, DOI: **10.1088/1755-1315/371/4/042022**.

7 D. Henkensmeier, M. Najibah, C. Harms, J. Žitka, J. Hnát and K. Bouzek, Overview: State-of-the art commercial membranes for anion exchange membrane water electrolysis, *J. Electrochem. Energy Convers. Storage*, 2021, **18**, 024001, DOI: **10.1115/1.4047963**.

8 M. Schalenbach, W. Lueke and W. L. D. Stolten, Hydrogen Diffusivity and Electrolyte Permeability of the Zirfon PERL Separator for Alkaline Water Electrolysis, *J. Electrochem. Soc.*, 2016, **163**, F1480–F1488, DOI: **10.1149/2.1251613jes**.

9 M. Suermann, A. Patru, T. J. Schmidt and F. N. Büchi, High pressure polymer electrolyte water electrolysis: Test bench development and electrochemical analysis, *Int. J. Hydrogen Energy*, 2017, **42**, 12076–12086, DOI: **10.1016/j.ijhydene.2017.01.224**.

10 N. Nambi Krishnan, D. Henkensmeier, J. H. Jang and H.-J. Kim, Nanocomposite Membranes for Polymer Electrolyte Fuel Cells, *Macromol. Mater. Eng.*, 2014, **299**, 1031–1041, DOI: **10.1002/mame.201300378**.

11 K. D. Kreuer, On the development of proton conducting polymer membranes for hydrogen and methanol fuel cells, *J. Membr. Sci.*, 2001, **185**, 29–39, DOI: **10.1016/S0376-7388(00)00632-3**.

12 X. Luo, S. Rojas-Carbonell, Y. Yan and A. Kusoglu, Structure-transport relationships of poly(aryl piperidinium) anion-exchange membranes: Eeffect of anions and hydration, *J. Membr. Sci.*, 2020, **598**, 117680, DOI: **10.1016/j.memsci.2019.117680**.

13 E. M. Schibli, J. C. Stewart, A. A. Wright, B. Chen, S. Holdcroft and B. J. Frisken, The Nanostructure of HMT-PMBI, a Sterically Hindered Ionene, *Macromolecules*, 2020, **53**, 4908–4916, DOI: **10.1021/acs.macromol.0c00978?ref=pdf**.

14 D. Aili, M. K. Hansen, R. F. Renzaho, Q. Li, E. Christensen, J. O. Jensen and N. J. Bjerrum, Heterogeneous anion conducting membranes based on linear and crosslinked KOH doped polybenzimidazole for alkaline water electrolysis, *J. Membr. Sci.*, 2013, **447**, 424–432, DOI: **10.1016/j.memsci.2013.07.054**.

15 J. O. Jensen, D. Aili, M. K. Hansen, Q. Li, N. J. Bjerrum and E. Christensen, A Stability Study of Alkali Doped PBI Membranes for Alkaline Electrolyzer Cells, *ECS Trans.*, 2014, **64**, 1175–1184, DOI: **10.1149/06403.1175ecst**.

16 D. Aili, K. Jankova, J. Han, N. J. Bjerrum, J. O. Jensen and Q. Li, Understanding ternary poly(potassium benzimidazolide)-based, *Polymer*, 2016, **84**, 304–310, DOI: **10.1016/j.polymer.2016.01.011**.

17 D. Aili, A. G. Wright, M. R. Kraglund, K. Jankova, S. Holdcroft and J. O. Jensen, Towards a stable ion-solvating polymer electrolyte for advanced alkaline water electrolysis, *J. Mater. Chem. A*, 2017, **5**, 5055–5066, DOI: **10.1039/c6ta10680c**.

18 M. R. Kraglund, D. Aili, K. Jankova, E. Christensen, Q. Li and J. O. Jensen, Zero-Gap AlkalineWater Electrolysis Using Ion-Solvating Polymer Electrolyte Membranes at Reduced KOH Concentrations, *J. Electrochem. Soc.*, 2016, **163**, F3125–F3131, DOI: **10.1149/2.0161611jes**.

19 D. Aili, K. Jankova, Q. Li, N. J. Bjerrum and J. O. Jensen, The stability of poly(2,2'-(m-phenylene)-5,5'-bibenzimidazole) membranes in aqueous potassium hydroxide, *J. Membr. Sci.*, 2015, **492**, 422–429, DOI: **10.1016/j.memsci.2015.06.001**.

20 M. R. Kraglund, M. Carmo, G. Schiller, S. A. Ansar, D. Aili, E. Christensen and J. O. Jensen, Ion-solvating membranes as a new approach towards high rate alkaline electrolyzers, *Energy Environ. Sci.*, 2019, **12**, 3313–3318, DOI: **10.1039/c9ee00832b**.

21 A. Konovalova, H. Kim, S. Kim, A. Lim, H. S. Park, M. R. Kraglund, D. Aili, J. H. Jang, H.-J. Kim and D. Henkensmeier, Blend membranes of polybenzimidazole and an anion exchange ionomer (FAA3) for alkaline water electrolysis: Improved alkaline stability and conductivity, *J. Membr. Sci.*, 2018, **564**, 653–662, DOI: **10.1016/j.memsci.2018.07.074**.

22 H. Penchev, G. Borisov, E. Petkucheva, F. Ublekov, V. Sinigersky, I. Radev and E. Slavcheva, Highly KOH doped para-polybenzimidazole anion exchange membrane and its performance in Pt/TinO2n−1 catalyzed water electrolysis cell, *Mater. Lett.*, 2018, **221**, 128–130, DOI: **10.1016/j.matlet.2018.03.094**.

23 L. A. Diaz, R. E. Coppola, G. C. Abuin, R. Escudero-Cid, D. Herranz and P. Ocón, Alkali-doped polyvinyl alcohol – Polybenzimidazole membranes for alkaline water electrolysis, *J. Membr. Sci.*, 2017, **525**, 45–55, DOI: **10.1016/j.memsci.2017.04.021**.

24 L. A. Diaz, J. Hnat, N. Heredia, M. M. Bruno, F. A. Viva, M. Paidar, H. R. Corti, K. Bouzek and G. C. Abuin, Alkali doped poly (2,5-benzimidazole) membrane for alkaline water electrolysis: Characterization and performance, *J. Power Sources*, 2016, **312**, 128–136, DOI: **10.1016/j.jpowsour.2016.02.032**.

25 W. Germer, J. Leppin, C. N. Kirchner, H. Cho, H.-J. Kim, D. Henkensmeier, K.-Y. Lee, M. Brela, A. Michalak and A. Dyck, Phase Separated Methylated Polybenzimidazole (O-PBI) Based Anion Exchange Membranes, *Macromol. Mater. Eng.*, 2015, **300**, 497–509, DOI: **10.1002/mame.201400345**.

26 M. Jung, W. Lee, C. Noh, A. Konovalova, G. S. Yi, S. Kim, Y. Kwon and D. Henkensmeier, Blending polybenzimidazole with an anion exchange polymer increases the efficiency of vanadium redox flow batteries, *J. Membr. Sci.*, 2019, **580**, 110–116, DOI: **10.1016/j.memsci.2019.03.014**.

27 L. Wang, A. T. Pingitore, W. Xie, Z. Yang, M. L. Perry and B. C. Benicewicz, Sulfonated pbi gel membranes for redox flow batteries, *J. Electrochem. Soc.*, 2019, **166**, A1449–A1455, DOI: **10.1149/2.0471908jes**.

28 L. Gubler, Membranes and separators for redox flow batteries, *Curr. Opin. Electrochem.*, 2019, **18**, 31–36, DOI: **10.1016/j.coelec.2019.08.007**.

29 C. Noh, D. Serhiichuk, N. Malikah, Y. Kwon and D. Henkensmeier, Optimizing the performance of meta-polybenzimidazole membranes in vanadium redox flow batteries by adding an alkaline pre-swelling step, *Chem. Eng. J.*, 2021, **405**, 126574, DOI: **10.1016/j.cej.2020.126574**.

30 H. Vogel and C. S. Marvel, *J. Polym. Sci.*, 1961, **50**, 511–539.

31 D. Aili, J. Yang, K. Jankova, D. Henkensmeier and Q. Li, From polybenzimidazoles to polybenzimidazoliums and polybenzimidazolides, *J. Mater. Chem. A*, 2020, **8**, 12854–12886, DOI: **10.1039/d0ta01788d**.

32 N. Nambi Krishnan, N. M. H. Duong, A. Konovalova, J. H. Jang, H. S. Park, H. J. Kim, A. Roznowska, A. Michalak and D. Henkensmeier, Polybenzimidazole/tetrazole-modified poly(arylene ether) blend membranes for high temperature proton exchange membrane fuel cells, *J. Membr. Sci.*, 2020, **614**, 118494, DOI: **10.1016/j.memsci.2020.118494**.

33 Q. Li, R. He, R. W. Berg, H. A. Hjuler and N. J. Bjerrum, Water uptake and acid doping of polybenzimidazoles as electrolyte membranes for fuel cells, *Solid State Ionics*, 2004, **168**, 177–185, DOI: **10.1016/j.ssi.2004.02.013**.

34 D. Aili, M. K. Hansen, J. W. Andreasen, J. Zhang, J. O. Jensen, N. J. Bjerrum and Q. Li, Porous poly(perfluorosulfonic acid) membranes for alkaline water electrolysis, *J. Membr. Sci.*, 2015, **493**, 589–598, DOI: **10.1016/j.memsci.2015.06.057**.

35 M. Najibah, E. Tsoy, H. Khalid, Y. Chen, Q. Li, C. Bae, J. Hnat, M. Plevova, K. Bouzek, J. H. Jang, H. S. Park and D. Henkensmeier, PBI nanofiber mat-reinforced anion exchange membranes with covalently linked interfaces for use in water electrolysers, *J. Membr. Sci.*, 2021, **640**, 119832, DOI: **10.1016/j.memsci.2021.119832**.

36 J. S. Yang, L. N. Cleemann, T. Steenberg, C. Terkelsen, Q. Li, J. O. Jensen, H. A. Hjuler, N. J. Bjerrum and R. He, *Fuel Cells*, 2014, **14**, 7–15, DOI: **10.1002/fuce.201300070**.

37 Y. Wang, S. N. Raskeev, J. R. Klaehn, C. J. Orme and E. S. Peterson, Interaction of gas molecules with crystalline polymer separation membranes: Atomic-scale modeling and first-principles calculations, *J. Membr. Sci.*, 2011, **384**, 176–183, DOI: **10.1016/j.memsci.2011.09.020**.

38 E. Babcock, N. Szekely, A. Konovalova, Y. Lin, M. S. Appavou, G. Mangiapia, Z. Revay, C. Stieghorst, O. Holderer, D. Henkensmeier, W. Lehnert and M. Carmo, Using neutron methods SANS and PGAA to study evolution of structure and composition of alkali-doped polybenzimidazole membranes, *J. Membr. Sci.*, 2019, **577**, 12–19, DOI: **10.1016/j.memsci.2019.01.026**.

39 K. A. Perry, K. L. More, E. A. Payzant, R. A. Meisner, B. G. Sumpter and B. C. Benicewicz, A Comparative Study of Phosphoric Acid-Doped m-PBI Membranes, *J. Polym. Sci., Part B: Polym. Phys.*, 2014, **52**, 26–35, DOI: **10.1002/polb.23403**.

40 L. Zhu, M. T. Swihart and H. Lin, Unprecedented size-sieving ability in polybenzimidazole doped with polyprotic acids for membrane H_2/CO_2 separation, *Energy Environ. Sci.*, 2018, **11**, 94–100, DOI: **10.1039/C7EE02865B**.

41 J. A. Wereta, M. T. Gehatia and D. R. Wiff, Morphological and Physical Property Effects for Solvent Cast Films of Poly-2, 5(6) Benzimidazole, *Polym. Eng. Sci.*, 1978, **18**, 204–209, DOI: **10.1002/pen.760180306**.

42 B. Singh, N. M. H. Duong, D. Henkensmeier, J. H. Jang, H. J. Kim, J. Han and S. W. Nam, Influence of different side-groups and cross-links on phosphoric acid doped radel based polysulfone membranes for high temperature polymer electrolyte fuel cells, *Electrochim. Acta*, 2017, **224**, 306–313, DOI: **10.1016/j.electacta.2016.12.088**.

43 X. Zhao, L. Song, J. Fu, P. Tang and F. Li, Experimental and DFT investigation of surface degradation of polyvinylidene fluoride membrane in alkaline solution, *Surf. Sci.*, 2011, **605**, 1005–1015, DOI: **10.1016/j.susc.2011.02.022**.

44 L. Xu, Y. Yu, W. Li, Y. You, W. Xu and S. Zhang, The influence of manufacturing parameters and adding support layer on the properties of Zirfon® separators, *Front. Chem. Sci. Eng.*, 2014, **8**, 295–305, DOI: **10.1007/s11705-014-1433-y**.

45 P. Vermeiren, W. Adriansens, J. P. Moreels and R. Leysen, The composite zirfon® separator for alkaline water electrolysis, in *Hydrogen Power: Theoretical and Engineering Solutions*, ed. T. O. Saetre, Springer Science + Business Media, Dordrecht, 1998, pp. 179–184, DOI: **10.1007/978-94-015-9054-9**.

46 S. Siracusano, S. Trocino, N. Briguglio, V. Baglio and A. S. Aricò, Electrochemical Impedance Spectroscopy as a Diagnostic Tool in Polymer Electrolyte Membrane Electrolysis, *Materials*, 2018, **11**, 1368, DOI: **10.3390/ma11081368**.

47 D. Zhang and K. Zeng, Evaluating the behavior of electrolytic gas bubbles and their effect on the cell voltage in alkaline water electrolysis, *Ind. Eng. Chem. Res.*, 2012, **51**, 13825–13832, DOI: **10.1021/ie301029e**.

48 J. Brauns, J. Schönebeck, M. Rykær Kraglund, D. Aili, J. Hnát, J. Žitka, W. Mues, J. O. Jensen, K. Bouzek and T. Turek, Evaluation of Diaphragms and Membranes as Separators for Alkaline Water Electrolysis, *J. Electrochem. Soc.*, 2021, **168**, 014510, DOI: **10.1149/1945-7111/abda57**.

49 T. Höfner, Development of Membrane Electrode Assemblies for the Anion Exchange Membrane Water Electrolysis, PhD thesis, 2016, RWTH Aachen University, **https://publications.rwth-aachen.de/record/661803/files/661803.pdf**.